

# Responses to reviews of “How does turbulence change approaching a rotor?” by Mann et al. wes-2017-53

Jakob Mann

April 23, 2018

We have received four reviews and comments which are addressed in chronological order. All changes to the manuscript are clearly marked in the attached version.

## 1 Comment by M. Pedersen

*On page 1, line 22-23 you write that Simley et al. (2016) see a slight rotation of the inflow in front of the rotor”*

*As I understand Simley et al. (2016), they see the rotation behind the rotor. Upstream they also see a slightly positive w-component, but they explain it as “due to the gently sloping nature of the terrain between the fjord and the V27.” See also page 1-9 in “Basismateriale for beregning af propelvindmøller” (link) which says there is no way the tangential force can affect the upstream flow because there, in practice, is no internal friction in the air.*

It is correct as Pedersen states that the vertical component of the flow measured in front of the rotor in Simley *et al* 2016 is not likely to be due to rotation. The flow was only measured in front of one half of the rotor and it more likely to be due to terrain effect. We have removed that statement from the paper and thank M. P. for the correction.

## 2 Review by M. Graham

*This is a very interesting paper as there is not much previously published showing measurements of the turbulent velocity field and spectra in the in-flow region of a full- scale HAWT together with numerical simulations which resolve the main blockage and distortion effects on the turbulent in-flow. The results are particularly interesting because they show clearly that the spectral power of the streamwise turbulent velocity component ( $u$ ) at low frequencies and below-rated wind speeds where the induction factor is large, reduces significantly as the rotor disc is approached while the power at high frequencies changes much less. This*

is seen in both the measurements and the accompanying LES computations. In a recent paper, commented on in the present paper, [Rapid distortion of turbulence into an open turbine rotor, Graham, JFM 2017], RDT theory is shown to predict a strong amplification of the spectral power of  $u$  at low frequencies as the rotor disc is approached, increasingly so the smaller the length-scale of the turbulence. At high frequencies the amplification reduces to insignificance. As observed by the authors in section 2.2 of the present paper this difference is most likely because the RDT calculation does not include the unsteady potential flow blocking effect of the rotor. This was excluded deliberately because the RDT calculations were intended to provide a correction for the incident turbulence velocity boundary condition used by lower fidelity computations which assume that the turbulence arrives ‘frozen’ at the rotor disc. The quasi-steady (QS) theory presented in the present paper to calculate the effects on the low frequency turbulence is an example of this and it is observed that it tends to over-predict the reduction. As is commented at the end of the present paper this may be because the amplification due to distortion is missing and that better agreement might be obtained if the RDT distortion correction were to be combined with the QS theory. The prediction of very little amplification or reduction of the spectral power of  $u$  at high frequency may be consistent similarly. Although the RDT predicts insignificant distortion in this region the unsteady potential blocking field also falls off with increasing rapidity ahead of the rotor disc for components of increasing frequency. These comments all refer to the below-rated results. It is more difficult to be sure why the power spectra of  $u$  in the in-flow clearly show considerable amplification in above-rated conditions in both the measured data and in the LES computations. In above-rated conditions the induction factor is considerably smaller and while the resulting blocking action reducing the power in the  $u$ -component is less, the effect of smaller induction factor is also to cause the distortion amplification to be much smaller. As said above this is an interesting paper presenting good quality results which I hope will stimulate further analysis on the topic of inflow turbulence.

We are happy for all the positive comments and also the consideration on combining the RDT and QS theories. We are eager to explore this combination in future work as we believe that Graham’s work really has opened for future opportunities to apply RDT.

### 3 Comment by A. Meyer Forsting

*Would it be possible to add the experimental results to Figure 7?*

This is a good suggestion. We have changed figure 7 to include low-frequency spectral ratios obtained from the measurements at  $\xi = -1.06$ . It shows good comparison between measurements, LES and the theory.

### 4 Review by anonymous Referee #2

*This is an interesting paper that pursues a clearly stated question of significant interest: how is turbulence modified at the rotor as compared to the incoming turbulence. The idea to use Rapid Distortion Theory (RDT) is solid and appropriate for the task at hand. The results presented are of interest. An initial aspect of the paper requires clearer explanation and justification. As it is now, the initial discussion separates between slow and rapid turbulence motions, and makes the claim that RDT can be applied to the higher-frequency fluctuations but it seems to imply that RDT should not be applicable to the slow incoming, larger, slower eddies. (I am referring to the first sentence in 2.2 “Rapid distortion theory for smaller turbulent scales corresponding to more rapid fluctuations is investigated by Batchelor and Proudman.”) This is contrary to the known limits of validity of RDT, which assume that if one moves with the turbulence but the mean flow varies very, very fast compared to the turbulence, then the linearization can be justified to represent the response of the SLOW LARGE eddies. So one expects RDT to work BETTER for the slow, bigger eddies of the inflow turbulence rather than the fast ones since their intrinsic scales are slower and they cannot “nonlinearly react” to the sudden change of flow conditions. The rapid eddies (small ones) can, on the other hand, nonlinearly relax more quickly to the rapid distortion from the rotor and adjust in nonlinear fashion thus violating the fundamental conditions of RDT-validity. It is possible that the authors mean different things when they say “slow” and “large..” and “small”. So, I would like to ask that they provide quantitative justification for applicability of RDT by quoting appropriately the ratio of relevant time-scales. Another aspect that is worthwhile pointing out is to better clarify what is the relationship between this work and RDT when the mean flow undergoes rapid “Axisymmetric expansion (one contracting + 2 expanding direction). This is a tricky case for RDT and turbulence modeling, see original papers Lee 1989 Phys. Fluids A 1, 1541–1557.*

*Details:*

*In Figure 7, clearly the LES data are all around 1, and the theory too except for the peak near 11.5 m/s for  $\xi = 0$ . In order to more clearly compare LES to the theory, why are there no LES done for  $U_\infty = 11.5$ ?*

Thank you for the positive comment and for pointing out that the discussion on the applicability of RDT is half misleading and half absent. We agree that careful assessment of the temporal and spatial scales should be performed in this paper.

Therefore, we have added a detailed explanation section 2.2 and also changed the header of that section (see the attached new version of the manuscript). It shows that only eddies that are smaller than a meter or so are not effectively “frozen” while experiencing the distortion by the induction zone.

We have included a reference to Lee (1989) stating that his results are in principle included in the analysis by Graham (2017) and they also do not take into account the interaction of the vorticity and the rotor because it is absent in his analysis.

Finally we have conducted yet an LES for  $U_\infty = 11.5$  m/s as suggested by the reviewer and included the results in figures 6 and 7. The simulations indeed

peak around 11.5 m/s although at a much lower value.

# How does turbulence change approaching a rotor?

Jakob Mann, Alfredo Peña, Niels Troldborg, and Søren J. Andersen

DTU Wind Energy, Technical University of Denmark

*Correspondence to:* J. Mann (jmsq@dtu.dk)

**Abstract.** For load calculations on wind turbines it is usually assumed that the turbulence approaching the rotor does not change its statistics as it goes through the induction zone. We investigate this assumption using a nacelle-mounted forward-looking pulsed lidar that measures low frequency wind fluctuations simultaneous at distances between one half and three rotor diameters upstream. The measurements show that below rated wind speed the low-frequency wind variance is reduced by up to 10% at one half rotor diameter upstream and above rated enhanced by up to 20%. A quasi-steady model that takes into account the change of thrust coefficient with wind speed explains these variations partly. Large-eddy simulations of turbulence approaching an actuator disk model of a rotor support the finding that the slope of the thrust curve influences the low-frequency fluctuations.

## 1 Introduction

10 It is routinely and often implicitly assumed in load calculations on wind turbines that the statistics of the turbulence does not change as the flow is approaching the rotor plane. As it is well known that the rotor affects the mean flow in front of the rotor it cannot be ruled out that also the turbulence is affected. In this paper we investigate this assumption experimentally with lidar measurements and large eddy simulation and compare the results with a simple model. We focus on low-frequency wind speed fluctuations.

15 Branlard et al. (2016) use vortex particle methods to calculate the effect of the turbine rotor on the incoming turbulence. They calculate the turbulent spectra at several center-line positions upstream of a Nordtank 500 kW wind turbine assuming a fixed thrust coefficient. They conclude that the presence of the rotor does not affect the turbulence spectrum significantly. However, at higher frequencies, above 0.1 Hz, they observe a slight decrease of the power spectral density when the presence of the rotor is taken into account implying marginally lower loads. They see no changes at lower frequencies. Branlard et al.  
20 (2016) emphasize that further investigations are necessary to conclude whether the effects of the stagnation on the turbulence are systematic or not (see also Branlard, 2017, which is an expanded version of Branlard's thesis).

Simley et al. (2016) measure the turbulent inflow towards a Vestas V27 wind turbine using three synchronized continuous wave, scanning Doppler lidars. They clearly see the stagnation in front of the rotor ~~and also a slight rotation of the inflow~~. The standard deviation of the along-wind velocity component  $\sigma_u$  decreases slightly close to the rotor plane and they hypothesize  
25 that this is linked to the reduced mean velocity, which also affects the low frequency fluctuations. They do not support this suggestion with spectral analysis and they also point out that the amount of data is limited. An additional complication is that

the Doppler lidars average the turbulent flow field in ways that depend on the direction from the lidars to the measurement volumes and their distances.

The change in the turbulence spectrum due to the stagnation in front of the rotor is investigated theoretically using rapid distortion theory by Graham (2017). In a first step, he assumes that the turbulent scales are much smaller than the size of the rotor. He also assumes that the mean flow around the rotor is described by the model of Conway (1995), a linearized actuator disk model, and that the approaching turbulence is isotropic and described by the von Kármán spectrum. With these assumptions, they derive that  $\sigma_u^2/\sigma_{u\infty}^2$  increases with the induction factor  $a$  of the rotor reaching a value of  $\sigma_u^2/\sigma_{u\infty}^2 \approx 1.34$  at the induction factor of maximal energy extraction  $a = 1/3$ . Here,  $\sigma_{u\infty}^2$  is the undisturbed, upstream variance of the longitudinal wind speed component  $u$  and  $\sigma_u^2$  is the local variance. He derives analytically that the amplification of turbulence is not equally distributed on frequencies but rather concentrated at lower frequencies leaving the inertial subrange almost unchanged. He also derives that the integral length scale of  $u$  in the  $y$ - or  $z$ -direction (i.e., perpendicular to the mean flow), which indicates how correlated fluctuations are across the rotor, increases as the flow approaches the rotor. The increase is a little less than the stretching by the mean flow in these perpendicular directions. Graham (2017) extends the theory to the more realistic case where the integral length of the turbulence is not much smaller than the rotor by concentrating on the flow along the symmetry line of the rotor. The amplification of  $\sigma_u^2$  is less for the small length scale case than cases with turbulence length scales of the order of or larger than the rotor. The amplification of  $\sigma_u^2/\sigma_{u\infty}^2$  decreases from 24% to 7% for  $a = 1/3$  as  $2L_u/D$  increases from 1 to 10, where  $L_u$  is the undisturbed integral length scale of  $u$  in the flow direction and  $D$  the rotor diameter. The variance slowly and asymptotically approaches its upstream value as  $L_u/D \rightarrow \infty$ .

Farr and Hancock (2014) perform wind tunnel model studies of the flow upstream of a rotor. They find very little change in  $\sigma_u$  approaching the rotor, much less than expected from the small scale rapid distortion limit discussed above. They suggest that the stagnation of the flow almost cancels out the amplification implied by rapid distortion theory.

In Sect. 2 we briefly discuss how quasi-steady fluctuations in the wind translate into fluctuations in the induction zone where we emphasize the effect of change in the induction with wind speed. That is followed by a discussion of a numerical experiment on turbulence in the induction zone in Sect. 3. Then we analyze a field experiment measuring low frequency variations in the induction zone with a pulsed Doppler lidar (Sect. 4). Finally, results are presented and discussed in Sects. 5 and 6.

## 2 Theory

The low frequency fluctuations is the focus of this paper and are discussed first. Then we summarize the results of Graham (2017), which should be valid for all frequencies but have a particularly simple solution for high frequencies. [Finally, we discuss the limitation of rapid distortion theory for our particular application.](#)

### 2.1 Quasi-steady fluctuations

Low-frequency or quasi-steady fluctuations are defined as variations in the wind speed  $U$  that are so slow that the rotor and the upstream flow has sufficient time to adjust to all the changes such that they appear as if the wind was steadily blowing at that

wind speed. If  $D = 2R = 100$  m and the induction zone extends  $3D$  upstream then the low frequency limit would be around  $f \approx 0.03$  Hz for a free mean wind speed  $U_\infty$  of 10 m/s.

For a particular wind turbine, the mean wind speed on a line extending upstream from the center of the rotor depends on the ambient wind speed  $U_\infty$  and the distance from the rotor normalized by the rotor radius  $\xi = x/R$  and is given by

$$5 \quad f(\xi, a, U_\infty) \equiv \frac{U}{U_\infty} = 1 - a \left( 1 + \frac{\xi}{\sqrt{1 + \xi^2}} \right). \quad (1)$$

A slow fluctuation in the ambient wind speed  $U_\infty$  will produce slow variations in the wind speed in the induction zone  $U(x)$ .

The power spectral density at low frequencies is therefore amplified as

$$\frac{S(x)}{S_\infty} = \left( \frac{\partial U}{\partial U_\infty} \right)^2 \quad (2)$$

where  $S(x)$  is the power spectral density (so the amplitude squared) at low frequencies at the position  $x$  and  $S_\infty$  is the upstream,

10 undisturbed spectrum. The partial derivative can be expanded as follows:

$$\frac{\partial U}{\partial U_\infty} = \frac{\partial f}{\partial U_\infty} U_\infty + f = f - \left( 1 + \frac{\xi}{\sqrt{1 + \xi^2}} \right) \frac{\partial a}{\partial U_\infty} U_\infty. \quad (3)$$

Typically,  $a$  does not change for ambient wind speeds below rated wind speed, so the second term is negligible. The spectral amplification in Eq. (2) will then be proportional to the square of relative slow down, which is of the order of but less than unity. Above rated,  $\partial a / \partial U_\infty$  will become negative and a positive amplification should be seen. A similar quasi-steady model

15 for how low frequency fluctuations of turbulence are modified by topography is presented by Mann (2000).

## 2.2 **Rapid-Small-scale fluctuations**

Rapid distortion theory (RDT) for smaller turbulent scales corresponding to more rapid fluctuations is investigated by Batchelor and Proudman (1954) and Townsend (1976). Townsend calculates the response of initially isotropic turbulence to a contraction (or expansion) of the mean flow, which to some extension is what is happening in front of a rotor. The theory is used in Graham

20 (2017) to produce amplifications of the velocity variance and the low frequency part of the velocity spectrum shown in Fig. 1.

The theory assumes that the vorticity lines are advected by the mean flow and that the approaching turbulence is isotropic as described in the Introduction and by Conway (1995). The theory implies that the amplification is strongest at the lowest frequencies and almost absent at the highest frequencies. Their results in the limit of turbulent scales much smaller than the rotor diameter are shown in Fig. 1. In a wind tunnel contraction, the  $u$ -component is diminished, also relative to the other

25 components. In contrast, the  $u$ -component is enhanced in the diverging flow in front of a rotor.

Now we analyze the applicability RDT by estimating the relevant spatial and temporal scales. The term "rapid" in RDT means that the turbulent eddies should not be able to interact during the time it takes for the distortion of the flow to take place. The eddies should not "rotate" several times during the distortion phase, in other words, their life-time  $\tau$  should be longer than the distortion time  $\mathcal{T}_D$ :

$$30 \quad \mathcal{T}_D \ll \tau \quad (4)$$

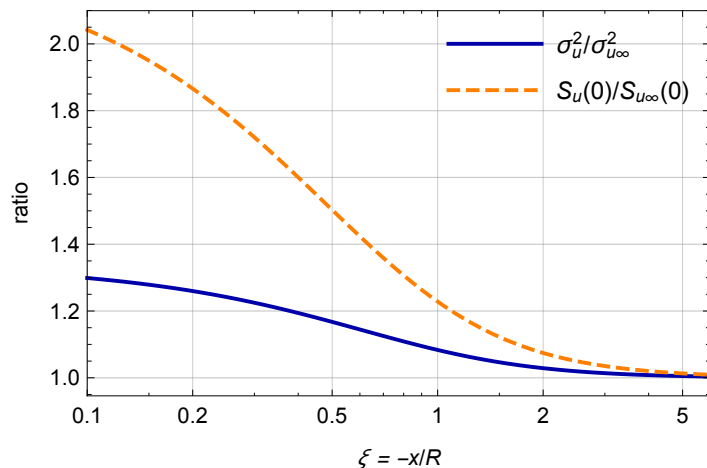


**Figure 1.** Amplification of the low-frequency spectrum and variance of longitudinal turbulence in the center of the rotor plane according to rapid distortion theory in the limit where the length scale of the turbulence is much smaller than the rotor radius. The induction factor is  $a = 1/3$ .

Another requirement for traditional RDT (Batchelor and Proudman, 1954; Townsend, 1976) but not for the work by Graham (2017) is that the shear or strain deforming the eddies is constant over the extent of the eddy. The strain changes appreciably in the wind turbine inflow zone over a length of the order of the size of the turbine, say its diameter  $D$ , so

$$D \ll k^{-1} \quad (5)$$

- 5 where we use the inverse wavenumber to characterize the size of the eddy. We now estimate the terms in Eqs. (4) and (5) to get a sense of applicable frequency or wavenumber ranges of traditional RDT. We estimate the distortion time scale as  $\mathcal{T}_D \approx D/U$  where  $U$  is the mean wind speed at hub height. In the work by Mann (1994) the simplest model for the eddy life-time in the neutral atmospheric surface-layer was

$$\tau = \Gamma \left( \frac{dU}{dz} \right)^{-1} (kL)^{-2/3} \quad (6)$$

- 10 where  $\Gamma$  is a constant of the order of 3,  $L$  is a length scale representative of the energy containing eddies, and  $dU/dz$  the shear at hub height. The model implies that small eddies (large  $k$ ) have a shorter life-time than larger eddies, so it is in the limit of small eddies that RDT has a limitation. The same eddy life-time model was used to extend the model by Mann (1994) to a semi-Lagrangian model (de Mare and Mann, 2016). For simplicity, we assume a logarithmic wind profile  $U(z) = u_* / \kappa \log(z/z_0)$  (Wyngaard, 2010) so  $dU/dz = u_* / (\kappa z)$  and that the diameter of the rotor is close to the hub height
- 15 above the ground  $D \approx z$ . Then isolating  $k$  in Eq. (4) we get

$$k \ll \frac{(\Gamma \log(z/z_0))^{3/2}}{L} \approx 5 \text{m}^{-1} \quad (7)$$



where we assume a hub height of  $z = 80$  m, a roughness length of  $z_0 = 0.05$  m, and use IEC (2005) to get  $\Gamma = 3.9$  and  $L = 33.6$  m. This inequality states that only eddies smaller in scale than a meter, or so, will be short-lived enough not to feel the entire distortion in the induction zone. Eq. (5) implies  $k \gg 0.013 \text{ m}^{-1}$  so looking at Fig. 4 we conclude that traditional RDT should be valid for frequencies higher than the peak of the spectrum (most energy containing eddies) and all the way up to the highest frequencies measured. Having estimated the range of applicability of traditional RDT we now turn our attention to an extension of RDT to larger scales.

The novelty of Graham (2017) is that he succeeds in calculating the velocity spectrum and variance without assuming that the length scale of the longitudinal turbulence  $L_{u\infty}$  is much smaller than the rotor. Graham develops the theory of Hunt (1973) further and exploit cleverly the axisymmetry of the mean flow to make the calculations feasible. As function of  $L_{u\infty}/R$ , the low-frequency part of the velocity spectrum decays slowly to the ambient value after a small initial increase. This is in contrast to Eqs. (2) and (3), which predict a reduction of the velocity variance equal to  $f^2$  for below rated where  $\partial a/\partial U_\infty = 0$ . The cause of this difference is that Graham (2017) does not take into account the interaction of the vorticity lines with the actuator disk. The velocity field that a vorticity line induces will be non-zero at the rotor plane, particularly for turbulence scales larger than the rotor, and the actuator disk will reduce the fluctuation caused by this vorticity line near the rotor. The same is assumed in Lee (1989) on axi-symmetric expansion of turbulence because in that work there is no rotor to interact with after the expansion.

### 3 Numerical techniques

#### 3.1 Wind turbine model

The wind turbine rotor is modelled as an actuator disk (AD) using the implementation proposed by Réthoré et al. (2014). Meyer Forsting et al. (2017) use the same model to simulate the induction zone of a 500 kW turbine and validated their predictions with lidar measurements.

The thrust force per unit area applied on the disk is assumed uniform and given by:

$$\frac{dF_T}{dA} = \frac{1}{2} \rho C_T(U_\infty) U_\infty^2, \quad (8)$$

where  $\rho$  is the density of air and  $C_T(U_\infty)$  is the thrust coefficient as function of the free-stream velocity  $U_\infty$ . The free-stream velocity is the velocity that would be at the disk location if the disk was not present. This velocity is not known a priori in an unsteady turbulent setting and therefore it is convenient to express the loading of the rotor in terms of the velocity averaged over the rotor disk,  $U_{\text{disk}}$ . For this reason we define a modified thrust coefficient,  $C_T^*(U_{\text{disk}})$ , as function of the disc averaged velocity

$$C_T^*(U_{\text{disk}}) = C_T(U_\infty) \frac{U_\infty^2}{U_{\text{disk}}^2} \quad (9)$$

such that Eq. (8) becomes:

$$\frac{dF_T}{dA} = \frac{1}{2} \rho C_T^*(U_{\text{disk}}) U_{\text{disk}}^2. \quad (10)$$

The  $C_T$  curve used in the present AD simulations is obtained from steady state simulations of the Siemens turbine presented by Troldborg and Meyer Forsting (2017) with a rated power of 2.3MW at 11.5 m/s. From their simulations, we also extract the relation between  $U_\infty$  and  $U_{\text{disk}}$  and thereby the  $C_T^*$  curve. Figure 2 shows the variation of  $C_T$  and  $C_T^*$  with respect to  $U_\infty$  and  $U_{\text{disk}}$ , respectively. As expected  $C_T^*$  reaches greater levels than  $C_T$  because  $U_{\text{disk}}$  is lower than  $U_\infty$ .

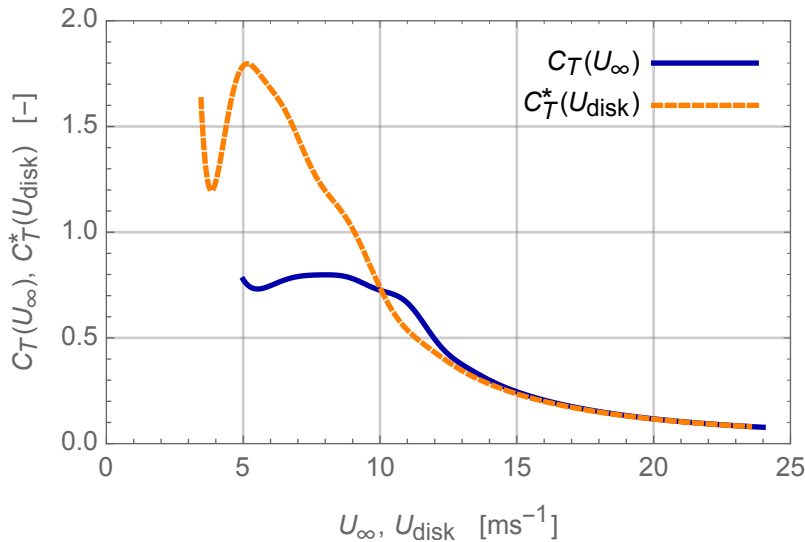


**Figure 2.** Thrust coefficient  $C_T$  and modified thrust coefficient  $C_T^*$  as functions of  $U_\infty$  and  $U_{\text{disk}}$ , respectively

5

The loading and power of the real Siemens turbine is controlled by regulating the rotational speed and pitch of the blades. The control essentially depends on the local flow conditions at the rotor disk. Thus, using  $U_{\text{disk}}$  to determine the load level at each instant in time is a simple method for mimicking the behaviour of the controller.

### 3.2 Computational domain

10 The computational domain is Cartesian and has dimensions  $(L_x, L_y, L_z) = (40R, 25R, 25R)$ , where  $L_x$ ,  $L_y$  and  $L_z$  are the domain length, width and height, respectively and  $R = 46.3$  m. The rotor is located in the center of the domain, i.e.  $(x, y, z) = (20R, 12.5R, 12.5R)$  with its center axis aligned with the  $x$ -direction (flow direction). The number of grid points in each direction of the domain is  $(N_x, N_y, N_z) = (320, 128, 128)$ . In the region defined by  $8.5R \leq x \leq 21.5R$ ,  $11.05R \leq y \leq 13.95R$  and  $11.05R \leq z \leq 13.95R$ , the grid cells are cubic with a side length of  $R/27.5$ . The reason for concentrating cells in this part  
15 of the domain is to better resolve the turbulent fluctuations in the region upstream of the rotor. Outside of this region, the cells are stretched towards the outer boundaries.

The boundary conditions are as follows: a fixed uniform velocity is prescribed at the inlet ( $x = 0$ ), bottom ( $z = 0$ ) and top

( $z = 25R$ ) boundaries. Periodic conditions are applied at the sides ( $y = 0$  and  $y = 25R$ ) and a zero gradient Neumann condition is applied to the velocity at the outlet ( $z = 40R$ ).

### 3.3 Turbulent inflow

The turbulent inflow is generated using the model of Mann (1994). The three parameters governing the Mann spectral tensor model are selected according to the findings of Peña et al. (2017), and represent the best fit to the measured conditions at Nørrekær Enge, which is the site of the lidar turbulence measurements. The output of the Mann simulation algorithm (Mann, 1998) is a spatial box of turbulent fluctuations, which are converted to time domain via Taylor’s frozen turbulence hypothesis. The dimensions of the generated box are  $(L_X, L_Y, L_Z) = (512R, 16R, 16R)$ , with a resolution of  $\Delta = R/8$ .

The turbulent fluctuations are introduced into the computational domain in a cross-section located  $8.25R$  upstream of the rotor using the technique described by Troldborg et al. (2014). Note, that only one quarter of the full cross-flow extent of the box is introduced in the simulations in order to avoid any influence of periodicity in the turbulence.

### 3.4 Flow solver and simulation set-up

The simulations are carried out using the incompressible Navier-Stokes flow solver EllipSys3D (Michelsen, 1992, 1994; Sørensen, 1995). EllipSys3D solves the finite volume discretized equations in general curvilinear coordinates utilizing a collocated grid arrangement. The code uses a modified Rhie-Chow algorithm (Réthoré and Sørensen, 2012; Troldborg et al., 2015) to avoid pressure velocity decoupling. The simulations are carried out as Detached Eddy Simulations (DES) using the  $k - \omega$  SST (Shear Stress Transport) model by Strelets (2001). The convective terms are discretized using a hybrid scheme, which switches between the Quadratic Upstream Interpolation for Convective Kinematics (QUICK) scheme (Leonard, 1979) in the Reynolds Averaged Navier Stokes (RANS) regions and a fourth-order central difference scheme in the large eddy simulation (LES) regions. The switching is determined through a limiter function given by Strelets (2001). The coupled momentum and pressure-correction equations are solved using the Semi-Implicit Method for Pressure Linked Equations (SIMPLE) algorithm (Patankar and Spalding, 1972). The solution is advanced in time using a second-order iterative time-stepping method using a time step of  $\Delta t = 0.08$  s. Simulations are carried out at free-stream velocities of  $U_\infty = 7, 8, 9, 11,$  and  $13$  m/s, respectively in order to cover operations both below and above rated wind speed. [In addition, we also do a simulation at 11.5 m/s where the amplification of the low-frequency fluctuations should peak.](#) Simulations are conducted both with and without a turbine included in the domain such that a one-to-one map in both space and time can be made of the influence of the rotor induction zone on the turbulence. The benefit of this approach is that it is insensitive to the distortion of the inserted turbulence, which is known to occur when the fluctuations are not in balance with the flow in which they are inserted.

## 4 Lidar experiment

The experiment took place at a 13 wind turbine farm in northern Denmark in generally flat terrain. A five-beam pulsed prototype lidar from Avent was mounted on the nacelle of a Siemens 2.3MW wind turbine with a hub height of 81.8 m and  $D =$

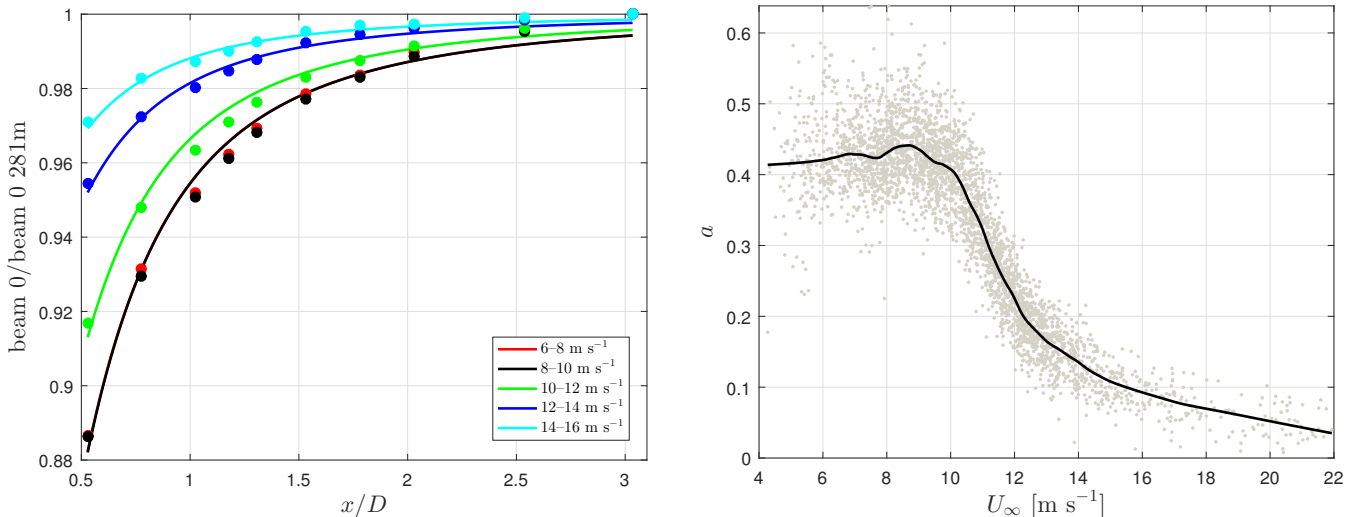


**Figure 3.** *Left:*  $U(x)/U_\infty$  as a function of the upstream distance from the rotor averaged over different intervals of  $U_\infty$ . The curves are fits to Eq. (1). *Right:* The induction factor  $a$  determined by fitting Eq. (1) to ten-minute means of the lidar measurements. The black curve is based on interval medians.

92.6 m. Only the central beam of the Avent lidar looking horizontally upstream of the turbine was used in this investigation. The lidar measured the line-of-sight velocity at ten range gates centered at 49, 72, 95, 109, 121, 142, 165, 188, 235, and 281 m upstream of the rotor at a sampling frequency of 0.2 Hz. All details about the experiment may be found in Peña et al. (2017).

## 5 Results

- 5 The line-of-sight velocity in the range gate centered around 235 m from the lidar and the wind speed from a WindSensor cup anemometer at the same distance and at hub height is compared to ensure the viability of the lidar. We find a slope deviating 1% from one and a correlation coefficient of 0.98. The scatter is larger than other similar comparisons (see for example Sathe et al., 2015, figure 4). Due to the yawing of the turbine, the measurements are rarely collocated. An additional difference between the measurements is that the cup measures the “wind way” (Kristensen, 1999) while the lidar measures the component of the
- 10 wind vector in the direction the wind turbine is pointing.

Having ensured the quality of the measurements we calculate the ten-minute average of the  $u$ -component of the wind and fit Eq. (1) to the measurements. That gives the value of  $a$  as a function of  $U_\infty$ , which we assume is equal to the velocity measured at the furthest range gate. The induction factors from the undisturbed sector (see Peña et al., 2017) are shown in Fig. 3 (right) together with a smooth curve through the points, which is later used to compute  $\partial a / \partial U_\infty$ . For wind speeds below

15 rated the induction factor reaches levels above 0.4 which is higher than the expected of approximately 0.3. The reason for this is that the quasi-steady model assumes a uniform load distribution and therefore tends to underestimate the induced velocity of real rotors which have a non-uniform loading, as shown by Troldborg and Meyer Forsting (2017). For a given  $C_T$ , this bias

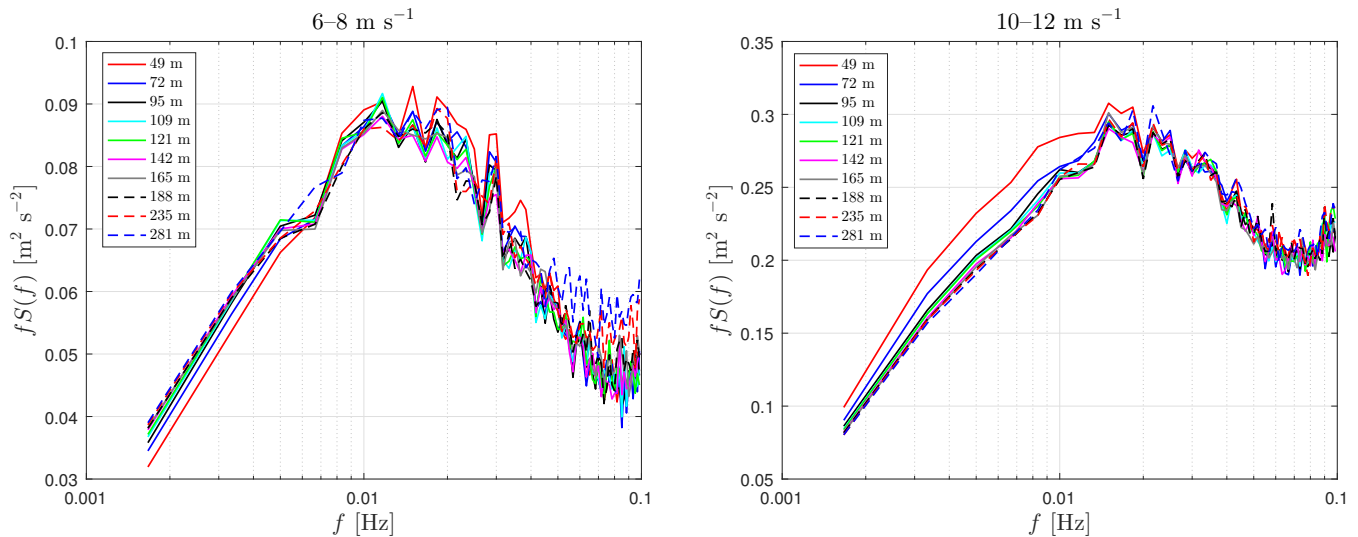


**Figure 4.** *Left:* Spectra of the line-of-sight velocity measured by the lidar as a function of up-stream distance to the rotor averaged over all measurements with  $6 < U_\infty < 8$  m/s. *Right:* The same, but for  $10 < U_\infty < 12$  m/s.

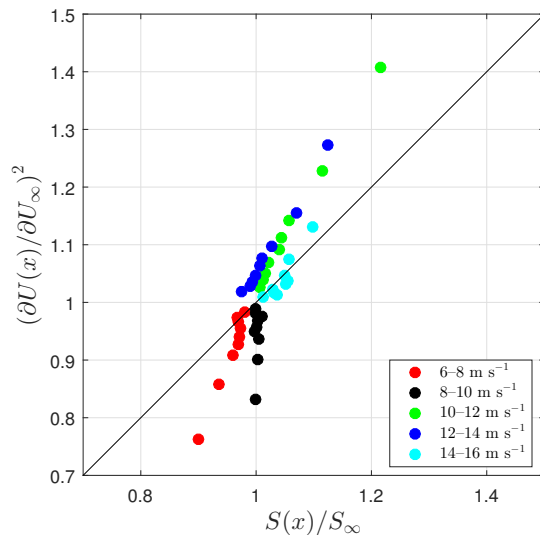


**Figure 5.** Change of low frequency ( $f < 0.007$  Hz) spectral power of the longitudinal velocity component measured by the lidar compared to  $(\partial U(x)/\partial U_\infty)^2$ . The different points for a given wind speed interval correspond to different distances from the rotor  $x$ .

causes an overestimation of the induction factor when the model is fitted to measurements of the upstream velocity. The bias is particularly dominant for the Siemens 2.3MW because it has a high local loading below rated wind speed, see Troldborg and Meyer Forsting (2017). Fig. 3 (left) shows values of the measured  $u(x)/U_\infty$  averaged in intervals of  $U_\infty$  with fits of Eq. (1) superimposed. It can be seen that the intervals below the rated wind speed  $6 < U_\infty < 8$  and  $8 < U_\infty < 10$  m/s almost coincide.

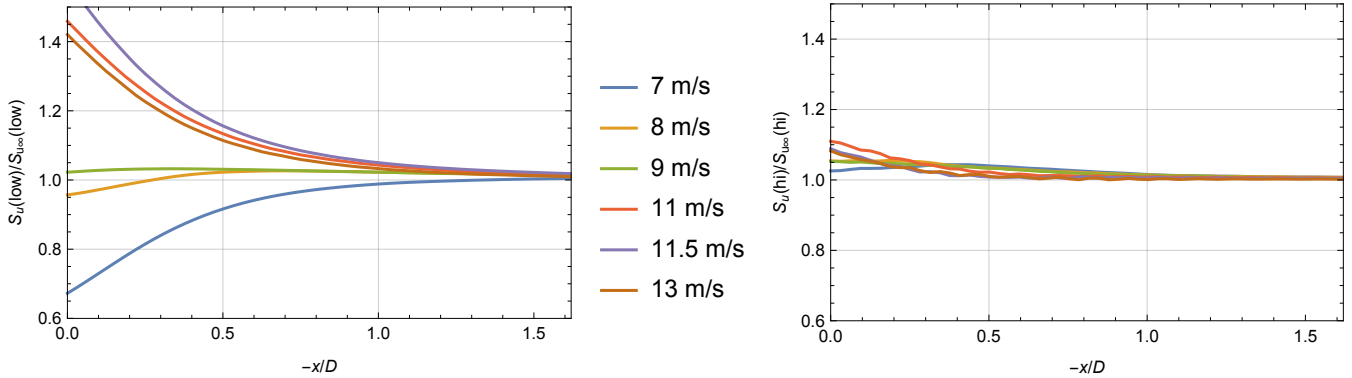


**Figure 6.** Low ( $f < 0.03$  Hz) and high ( $f > 0.03$  Hz) frequency variances from LES, left and right frames, respectively

We now calculate the power spectrum of the velocity at each range gate in all 2 m/s intervals of  $U_\infty$ . These are based on 10-minute time series so the lowest frequency investigated is  $f = 1/600\text{Hz} = 0.00167$  Hz. Two examples are shown in Fig. 4 for an  $U_\infty$  where  $a$  is constant with  $U_\infty$  and for a velocity where  $a$  rapidly decreases as a function of  $U_\infty$ . For low frequencies, the power spectra for the low  $U_\infty$  coincide for most ranges except for those closest to the rotor when they are slightly but significantly lower. Conversely, for the higher  $U_\infty$ , the spectra close to the rotor are significantly higher than the upstream spectra. The experiment has the great advantage that the measurements at all range gates are done simultaneously with the same instrument making detection of small differences possible.

The experimental results are summarized in Fig. 5. Here we calculate the low-frequency spectral amplification as measured by the lidar  $S_{\text{low}}(x)/S_{\text{low},\infty}$  where

$$10 \quad S_{\text{low}} \equiv \int_{1/600 \text{ Hz}}^{4/600 \text{ Hz}} S(f) df, \quad (11)$$

i.e. we add the four lowest frequency bins of the 10-minute average spectra. We calculate the low frequency fluctuations using different upper frequency limit. The results vary but the trend remains. On the [y-axis](#), we plot the expected amplification according to the quasi-steady model in Eq. (3) where the induction factor and its slope is derived from the solid curve in Fig. 3 (right). The cloud of points corresponding to each  $U_\infty$  bin are results from nine range gates (the tenth is used for normalization assuming it is far enough away to represent the ambient flow). The trend that the low-frequency fluctuations are reduced below rated and amplified above is captured but the exact magnitude is not.

We now turn to the analysis of the LES simulations. Since the turbulence is not completely homogeneous in the stream-wise direction, we determine the effect of the rotor on the fluctuations at a position  $x$  by comparing the two simulations with and without the rotor at that position. In Fig. 6 we show the relative changes of turbulence divided into low and high frequencies. At low frequencies the fluctuations below rated wind speed are reduced while they are amplified above rated. The high frequency fluctuations, or what the LES can resolve of them, change very little.

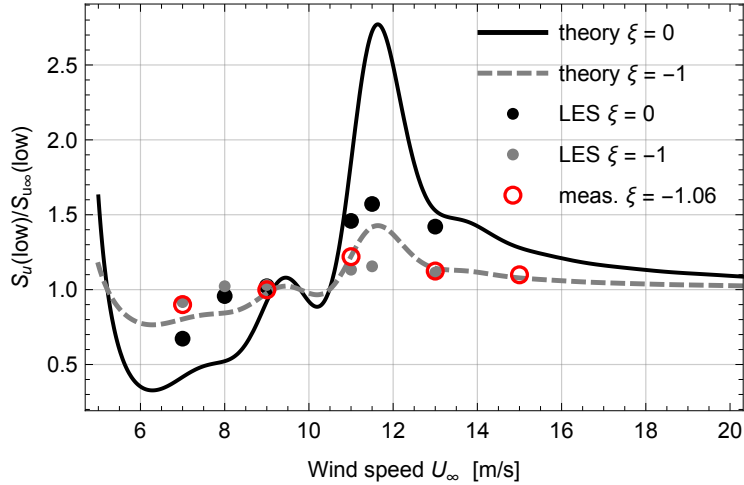


**Figure 7.** Change of low frequency ( $f < 0.03$  Hz) spectral power of the longitudinal velocity component in the rotor plane and one radius upstream. The dots are the LES simulations while the lines are the quasi-steady model based on Eqs. (2) and (3). [The circles are lidar measurements using Eq \(11\) at  \$\xi = -1.06\$ .](#)

In Fig. 7 we summarize the results and compare them with the quasi-steady model. The theoretical prediction is based on the thrust curve shown in Fig. 2. We put a fifth-order spline through the points to be able to do derivatives and then we use the relation

$$a = \frac{1}{2} \left( 1 - \sqrt{1 - C_T} \right) \quad (12)$$

5 to get the induction factor (Hansen, 2015). We are then able to use Eq. (3) to predict the change of low-frequency fluctuations. We do that for two distances from the rotor,  $x = 0$  and  $x = -R$ . Again the model has the trends right, but the magnitude, especially below rated is exaggerated.

Since the theory by Graham (2017) predicts an increase of low-frequency  $u$ -fluctuations near the rotor, a combination of the two models could potentially improve the results.

## 10 6 Conclusions

The often used assumption that the statistics of turbulence approaching a wind turbine rotor is unaltered relative to its upstream values is investigated in this paper. Since the mean wind speed is reduced in the induction zone one cannot rule out that the turbulence is also affected.

15 A nacelle-mounted forward-looking pulsed lidar is used to measure low frequency wind fluctuations upstream of a wind turbine rotor situated in flat, homogeneous terrain. It measures wind speeds simultaneously at ten ranges between one half and three rotor diameters upstream sampling at 0.2 Hz. The integral of the velocity spectrum up to a frequency of 1/150 Hz

is reduced by up to 10% at one half rotor diameter upstream and above rated enhanced by up to 20%. The changes disappear rapidly further upstream.

A quasi-steady model that uses the  $C_T$ -curve predicts partly the variation, but overestimates the changes. The model differs from a recent development of rapid distortion theory that is applicable also to low-frequency fluctuations (Graham, 2017).

- 5 An implementation of an actuator disk model in a large eddy simulation is used to investigate the changes in detail. The simulation is not completely homogeneous in the along-wind direction so the changes in turbulence statistics are found by comparing otherwise identical simulation runs with and without the rotor at corresponding positions. The simulations supports the finding that the slope of the thrust curve influences the low-frequency fluctuations but the simple quasi-steady model overestimates the changes. The exact consequences for loads are not investigated in this work.

- 10 *Author contributions.* JM wrote most of the manuscript except Sect. 3 which was written by NT. AP did the analysis of the lidar data, NT and SJA did the LES, JM analyzed the LES output and did the theory in Sect. 2. All authors commented on the manuscript.

*Acknowledgements.* This work is partly funded by the Unified Turbine Testing (UniTTe) project funded by The Innovation Fund Denmark (1305-00024B).



## References

- Batchelor, G. K. and Proudman, I.: The effect of rapid distortion of a fluid in turbulent motion, *Quart. J. Mech. Appl. Math.*, 7, 83–103, 1954.
- Branlard, E.: *Wind Turbine Aerodynamics and Vorticity-Based Methods: Fundamentals and Recent Applications*, vol. 7, Springer, 2017.
- Branlard, E., Mercier, P., Macheaux, E., Gaunaa, M., and Voutsinas, S.: Impact of a wind turbine on turbulence: Un-freezing turbulence by means of a simple vortex particle approach, *Journal of Wind Engineering and Industrial Aerodynamics*, 151, 37–47, 2016.
- 5 Conway, J. T.: Analytical solutions for the actuator disk with variable radial distribution of load, *Journal of Fluid Mechanics*, 297, 327–355, 1995.
- de Mare, M. and Mann, J.: On the Space-Time Structure of Sheared Turbulence, *Bound.-Layer Meteorol.*, <https://doi.org/DOI.10.1007/s10546-016-0143-z>, 2016.
- 10 Farr, T. D. and Hancock, P. E.: Torque fluctuations caused by upstream mean flow and turbulence, in: *Journal of Physics: Conference Series*, vol. 555, p. 012048, IOP Publishing, 2014.
- Graham, J. M. R.: Rapid distortion of turbulence into an open turbine rotor, *Journal of Fluid Mechanics*, 825, 764–794, 2017.
- Hansen, M. O.: *Aerodynamics of wind turbines*, Routledge, 2015.
- Hunt, J. C. R.: A theory of turbulent flow round two-dimensional bluff bodies, *J. Fluid Mech.*, 61, 625–706, 1973.
- 15 IEC: IEC 61400-1. Wind turbines – design requirements, International Electrotechnical Commission, 3 edn., 2005.
- Kristensen, L.: The Perennial Cup Anemometer, *Wind Energy*, 2, 59–75, 1999.
- Lee, M. J.: Distortion of homogeneous turbulence by axisymmetric strain and dilatation, *Phys. Fluids A*, 1, 1541, 1989.
- Leonard, B. P.: A stable and accurate convective modelling procedure based on quadratic upstream interpolation, *Comp. Meth. in Appl. Mech. and Engrng.*, 19, 59–98, 1979.
- 20 Mann, J.: The spatial structure of neutral atmospheric surface-layer turbulence, *J. Fluid Mech.*, 273, 141–168, 1994.
- Mann, J.: *Wind Field Simulation*, *Prob. Engng. Mech.*, 13, 269–282, 1998.
- Mann, J.: The spectral velocity tensor in moderately complex terrain, *J. Wind Eng. Ind. Aerodyn.*, 88, 153 – 169, 2000.
- Meyer Forsting, A., Troldborg, N., Murcia Leon, J., Sathe, A., Angelou, N., and Vignaroli, A.: Validation of a CFD model with a synchronized triple-lidar system in the wind turbine induction zone, *Wind Energy*, 20, 1481–1498, 2017.
- 25 Michelsen, J. A.: Basis3D – a platform for development of multiblock PDE solvers, Tech. Rep. AFM 92-05, Dept. of Fluid Mechanics, Technical University of Denmark, 1992.
- Michelsen, J. A.: Block structured multigrid solution of 2D and 3D elliptic PDEs, Tech. Rep. AFM 94-06, Dept. of Fluid Mechanics, Technical University of Denmark, 1994.
- Patankar, S. V. and Spalding, D. B.: A Calculation Procedure for Heat, Mass and Momentum Transfer in Three-Dimensional Parabolic Flows, *Int. J. Heat Mass Transfer*, 15, 1787–1972, 1972.
- 30 Peña, A., Mann, J., and Dimitrov, N.: Turbulence characterization from a forward-looking nacelle lidar, *Wind Energy Science*, 2, 133, 2017.
- Réthoré, P.-E. and Sørensen, N. N.: A discrete force allocation algorithm for modelling wind turbines in computational fluid dynamics, *Wind Energy*, 15, 915–926, 2012.
- Réthoré, P.-E., Laan, P., Troldborg, N., Zahle, F., and Sørensen, N. N.: Verification and validation of an actuator disc model, *Wind Energy*, 35 17, 919–937, 2014.
- Sathe, A., Mann, J., Vasiljevic, N., and Lea, G.: A six-beam method to measure turbulence statistics using ground-based wind lidars, *Atmospheric Measurement Techniques*, 8, 729–740, <https://doi.org/10.5194/amt-8-729-2015>, 2015.

- Simley, E., Angelou, N., Mikkelsen, T., Sjöholm, M., Mann, J., and Pao, L. Y.: Characterization of wind velocities in the upstream induction zone of a wind turbine using scanning continuous-wave lidars, *Journal of Renewable and Sustainable Energy*, 8, 013 301, 2016.
- Sørensen, N. N.: General Purpose Flow Solver Applied to Flow over Hills, PhD thesis Risø-R-864(EN), Risø National Laboratory, 1995.
- Strelets, M.: Detached eddy simulation of massively separated flows, in: 39th AIAA Aerospace sciences meeting and exhibit, p. 879, 2001.
- 5 Townsend, A. A.: *The Structure of Turbulent Shear Flow*, Cambridge University Press, 2nd edn., 1976.
- Troldborg, N. and Meyer Forsting, A. R.: A simple model of the wind turbine induction zone derived from numerical simulations, *Wind Energy*, 2017.
- Troldborg, N., Sørensen, J. N., Mikkelsen, R., and Sørensen, N. N.: A simple atmospheric boundary layer model applied to large eddy simulations of wind turbine wakes, *Wind Energy*, 17, 657–669, 2014.
- 10 Troldborg, N., Sørensen, N. N., Réthoré, P.-E., and van der Laan, M.: A consistent method for finite volume discretization of body forces on collocated grids applied to flow through an actuator disk, *Computers & Fluids*, 119, 197–203, 2015.
- Wyngaard, J. C.: *Turbulence in the Atmosphere*, Cambridge, 2010.